








Coordinated Beamforming Design for Multi-User Multi-Cell MIMO VLC Networks

Shimaa Naser , Lina Bariah , *Senior Member, IEEE*, Wael Jaafar , *Senior Member, IEEE*, Sami Muhaidat , *Senior Member, IEEE*, Mahmoud Al-Qutayri , *Senior Member, IEEE*, Murat Uysal , *Fellow, IEEE*, and Paschalis C. Sofotasios 

Abstract—Inter-cell interference (ICI) and inter-user interference (IUI) constitute a major issue towards achieving the optimum spectral efficiency (SE) and energy efficiency (EE) performance in multi-cell visible light communication (VLC) networks. Hence, advanced multiple access techniques need to be leveraged in order to improve the provided service to the users of such interfering networks. To this end, the present contribution proposes the integration of coordinated beamforming (CB) with rate-splitting multiple access (RSMA) in multi-cell VLC systems. Specifically, we consider the design of beamformers for the common and private streams in a coordinated manner between different attocells, which is shown to provide efficient mitigation of the incurred interference. Additionally, the formulated optimization problem aims to minimize the sum of the mean squared error across all attocells in order to jointly determine the optimum receive filters and coordinated transmit beamformers for RSMA streams. In this context, we illustrate through extensive computer simulations, which are carried out in a realistic setup that assumes noisy channel state information acquisition, the distinct flexibility and robustness of CB-based RSMA in mitigating the incurred interference. Finally, the offered results demonstrate the superiority of CB-based RSMA in terms of achievable SE and EE performance in multi-cell VLC

networks compared to the conventional CB-based space division multiple access counterpart.

Index Terms—Coordinated beamforming, MIMO, multicell communications, spectral efficiency, optimization, RSMA, energy efficiency, VLC.

I. INTRODUCTION

MODERN large-scale infrastructures are usually equipped with multiple illuminating devices, paving the way for the conceptualization of optical attocells, and hence, facilitating the deployment of low complexity visible light communication (VLC) systems. In addition to this, the attocells concept has been shown capable of providing ubiquitous indoor coverage in large indoor VLC environments [1], [2]. In such a configuration, each light emitting diode (LED) array in the attocell acts as a VLC access point (AP), that serves multiple user equipment (UE) devices within its coverage area. It is worth noting that the issue of achieving the optimal design of LEDs deployment is an important factor that guarantees both illumination and connectivity requirements. This is because a large number of attocells in a room is not preferable and can increase the interference among neighboring attocells. On the contrary, a small number of randomly deployed LED arrays may not satisfy the illumination and coverage requirements. For instance, in [3] two approaches were introduced, focusing on either minimizing the number of LEDs to be used in order to provide service requirements or maximizing the number of users to be served with a fixed number of LEDs. On the other hand, the authors in [4] proposed an LEDs arrangement design using 16 LED arrays in an indoor VLC system, aiming to increase light uniformity and decrease power and signal-to-noise ratio (SNR) fluctuations across the room without increasing number of LED arrays.

In the context of multi-cell configurations, UEs located at the cell-edge suffer from both inter-cell interference (ICI) and inter-user interference (IUI). In this context and in order to improve the performance of the cell-edge UEs, a variety of time/frequency/power coordination schemes have been proposed across the attocells [5]–[7]. More specifically, in [5], the authors attempted to optimize different parameters including the transmit power on carriers, precoders, and scheduling weights. Likewise, the authors in [6] and [7] considered resource allocation schemes for multi-cell cooperative/coordinated transmission. Within the same context, the authors in [8] proposed

Manuscript received March 21, 2022; revised April 11, 2022; accepted April 13, 2022. Date of publication April 21, 2022; date of current version May 19, 2022. This work was supported by Khalifa University under Grants KU/FSU-8474000122, KU/RC1-C2PS-8474000137/T2, and KU/RC1-C2PS-8474000137/T5. This work was presented in part at IEEE WCNC 2021, Nanjing, China. [DOI: 10.1109/WCNCW49093.2021.9419979]. (*Corresponding author: Paschalis C. Sofotasios.*)

Shimaa Naser and Lina Bariah are with the Center for Cyber-Physical Systems, Department of Electrical Engineering and Computer Science, Khalifa University, Abu Dhabi 127788, UAE (e-mail: 100049402@ku.ac.ae; lina.bariah@ieee.org).

Wael Jaafar is with the Department of Systems and Computer Engineering, Carleton University, Ottawa, ON K1S 5B6, Canada (e-mail: waeljaafar@sce.carleton.ca).

Sami Muhaidat is with the Center for Cyber-Physical Systems, Department of Electrical Engineering and Computer Science, Khalifa University, Abu Dhabi 127788, UAE, and also with the Department of Systems and Computer Engineering, Carleton University, Ottawa, ON K1S 5B6, Canada (e-mail: muhaidat@ieee.org).

Mahmoud Al-Qutayri is with the Systems-on-Chip Center, Department of Electrical Engineering and Computer Science, Khalifa University, Abu Dhabi 127788, UAE (e-mail: mahmoud.alqutayri@ku.ac.ae).

Murat Uysal is with the Department of Electrical and Electronics Engineering, Ozyegin University, 34794 Istanbul, Turkey (e-mail: murat.uysal@ozyegin.edu.tr).

Paschalis C. Sofotasios is with the Center for Cyber-Physical Systems, Department of Electrical Engineering and Computer Science, Khalifa University, Abu Dhabi 127788, UAE, and also with the Department of Electrical Engineering, Tampere University, 33014 Tampere, Finland (e-mail: paschalis.sofotasios@ku.ac.ae).

Digital Object Identifier 10.1109/JPHOT.2022.3169233

interference graph-based scheduling approaches and a bipartite graph-based scheduling approach to achieve higher user signal-to-interference-plus-noise ratio (SINR) and better fairness. Moreover, the authors in [9] investigated the optimization problem of subchannel and power allocation to maximize energy efficiency (EE) under transmit power and quality-of-service constraints. Likewise, [10] proposed joint cell formation and power allocation algorithms by formulating an optimization problem that aims at maximizing the corresponding EE. On the contrary, Zhou *et al.* proposed multi-color schemes for frequency reuse [11], which despite its advantages it degrades the illumination performance of the LEDs. This effect is also widely known as color rendering.

It is recalled that the performance of multiple access schemes has been also considered in VLC systems [12]–[18] and the references therein. To this effect, the investigation of orthogonal frequency division multiple-access (OFDMA) based on DC-biased optical (DCO)-OFDM in multi-cell VLC networks was considered in [19]. Similarly, a multi-carrier cooperating scheme was proposed in [20], where neighboring APs jointly coordinate their transmission using DCO-OFDM. Likewise, the authors in [21], [22] reported a novel multi-carrier based cell partitioning and frequency reuse scheme to mitigate ICI in VLC multi-cell systems. In contrast, Chen *et al.* proposed an ICI mitigation technique using optimized angle-diversity VLC receivers [23]. However, this approach requires major changes in the receiver's structure, which is complex to achieve in practice.

Typically, in large-scale VLC networks, the AP is composed of multiple interconnected LEDs to provide multiple-input multiple-output (MIMO) communication. In such a communication scenario, multi-user precoding needs to be leveraged in order to handle the incurred IUI and ICI [24]. To that end, an advanced precoding based strategy has been proposed for multi-cell MIMO VLC systems, known as coordinated multi-point (CoMP) transmission [25]. In a CoMP transmission, the APs of different attocells are connected through backbone links in order to provide a certain level of coordination/cooperation among them [26]. The simplest form of CoMP precoding is per-cell coordination scheme, where only the precoder values are shared between the attocells whilst the incurred ICI is treated as a noise. Hence, the precoder design and its associated optimization at the attocells is carried-out independently. Nevertheless, despite its simplicity and overall usefulness, per-cell coordination does not ultimately mitigate ICI [26]. Alternatively, joint transmission (JT) scheme has been shown to have efficient capabilities in mitigating inter-cell interference compared to per-cell coordinated precoding design by sharing all users' data and channel state information (CSI) between all cells. Therefore, attocells' boundaries are removed and the precoders design is carried-out collaboratively among different cells [26]. Nevertheless, JT faces several challenges, such as high complexity, AP-UEs synchronization, and limited bandwidth of backhaul links. Accordingly, coordinated beamforming (CB) was proposed with the aim to provide a compromised complexity and performance compared to JT. The distinct characteristic of CB is that only CSI is shared between attocells, whilst the precoders design at the corresponding cells is performed in a coordinated manner [27], [28]. It is worth noting that, the performance of CB-RSMA can

be improved through partial data sharing between the adjacent attocells. More specifically, since the used LEDs have limited coverage, interfering attocells are allowed to exchange the associated data streams of cell-edge users between the cell-edge LEDs on the borders that contribute to the majority of the ICI. Then, the set of the LEDs in the i^{th} attocell can cooperate with the cell-edge LEDs on the borders of the neighbouring attocells, to jointly serve the cell-edge users in the i^{th} attocell by transmitting their messages from the cell-edge LEDs of the interfering attocells in addition to the LEDs of the same attocell. Although partial cooperation is less restricted compared to JT, it still requires a little bit higher complexity and synchronization between adjacent attocells compared to CB-RSMA.

In the context of multiple access schemes, rate-splitting multiple access (RSMA) has been identified recently as a highly-reliable and spectrally-efficient scheme, which outperforms both non-orthogonal multiple access (NOMA) and multi-user linear precoding, also known as space-division multiple access (SDMA) [29]–[36]. In order to achieve a controlled level of interference in RSMA systems, the transmitted signal of each user is divided into one or several common parts, that are multiplexed with each other, and to a private part that is decoded only by the corresponding user. RSMA relies on linearly precoded rate-splitting along with the use of successive interference cancellation (SIC), in order to reliably decode part of the interference embedded in the common message and treat the remaining (other users' private messages) as noise.

Inspired by the promising capabilities of RSMA in the radio frequency (RF) domain, it is envisioned to bring several advantages in multi-cell VLC systems. Nevertheless, its application in the context of VLC is still in its infancy and only few contributions have addressed the integration of RSMA into VLC systems, such as [37]–[41]. However, the presented framework in [37][39] are limited to single-cell VLC networks, where it was demonstrated that RSMA outperforms both NOMA and SDMA in terms of achievable spectral efficiency (SE) and EE. On the other hand, the authors in [38] considered multi-cell RSMA in centralized VLC systems, where all attocells were treated as a single large cell. The presented RSMA framework in [38] has the same limitations associated with the aforementioned JT scheme. Recently, the authors in [40] have considered the integration of RSMA with multi-cell VLC systems, wherein the inter-cell interference was mitigated through zero-forcing (ZF) approach for the inter-cell region. However, ZF precoding has relatively degraded performance at low SNR regimes and when the number of the transmitting LEDs it is less than the total number of users of all the coordinated attocells.

To the best of the authors knowledge, no comprehensive framework that investigates the integration of RSMA into multi-cell VLC systems, while considering challenges pertaining to interference mitigation and complexity reduction, has been reported in the open technical literature. In this regard, motivated by the advantages offered by RSMA in single-cell systems and the capabilities of CB scheme to mitigate interference along with its reduced complexity, we propose the integration of CB with RSMA in multi-cell VLC networks. Our proposed scheme is expected to bring additional benefits in mitigating the incurred interference, while reducing the precoder design

complexity compared to centralized precoder design for RSMA. In specific, in this paper, we formulate an optimization problem that minimizes the sum of mean squared error (MSE) across all users in a multi-cell VLC network. The formulated problem aims to jointly find the optimum receive filters and coordinated beamformers for the common-private messages. This is carried out in a realistic setup where, in addition to considering the involved ICI and IUI, we assume noisy CSI acquisition, which is practically the case in realistic communication scenarios. Based on this and due to the non-convexity of the formulated optimization problem, we use the sub-optimal alternating optimization (AO) approach to solve it robustly and efficiently.

Capitalizing on the the above, the obtained results demonstrate the distinct flexibility and robustness of CB-based RSMA in mitigating the incurred interference. Additionally, CB-based RSMA exhibits a superior performance in terms of the SE and EE over conventional CB-based SDMA scheme for realistic channel state conditions. Importantly, this is achieved by also maintaining a reduced complexity compared to the centralized design of RSMA in multi-cell networks. More specifically, the contributions of the present work are summarized below:

- 1) We propose the integration of CB and RSMA for indoor multi-cell VLC systems. The proposed framework is expected to enhance the achievable SE and EE for various UEs' deployments and networks load.
- 2) We formulate a joint optimization of the receiver filters and transmit precoders with the aim to minimize the sum of MSE (SMSE) of all UEs. Motivated by the compromised performance and complexity offered by CB compared to JT and per-cell coordination, we utilize it to design the precoders of the common and private messages. Due to the non-convexity of the formulated optimization problem, we opt to use a sub-optimal AO algorithm to solve it robustly and efficiently.
- 3) Through the adoption of a noisy CSI model, we quantify the impact of the channel uncertainty on the CB design of the common and private messages, and demonstrate its importance in practical CB-based RSMA VLC network configurations.
- 4) Finally, we evaluate through extensive computer simulations the achievable performance of CB-based RSMA in terms of SE and EE. Furthermore, we compare the obtained results with baseline CB-based multiple access techniques such as SDMA. The offered results provide useful theoretical and practical insights that are anticipated to be useful in the design and deployment of efficient VLC networks.

The remainder of the paper is organized as follows: Section II presents the considered system model and the problem formulation, assuming imperfect CSI estimation. Then, Section III demonstrates thoroughly the proposed solution to this problem. The corresponding numerical and simulation results, along with discussions, are presented in Section IV. Finally, Section V concludes the paper with useful remarks.

Notations: Unless otherwise stated, boldface uppercase and lowercase represent matrices and vectors, respectively. Also,

$(\cdot)^T$ denotes the transpose operation, $\mathbb{E}(\cdot)$ represents the statistical expectation, $\|\cdot\|$ is the Euclidean norm, $|\cdot|$ is the absolute value, and $\text{Trac}(\mathbf{A})$ is the trace of a matrix \mathbf{A} . Also, assuming a vector $\mathbf{z} = [z_1, \dots, z_Z]$ with length Z , $L_1(\mathbf{z}) = \sum_{i=1}^Z |z_i|$ denotes the L_1 norm. Finally, $\mathbf{1}_{N \times 1}$ is the all-ones vector of size $N \times 1$, whereas I denotes the identity matrix.

II. SYSTEM MODEL AND PROBLEM FORMULATION

A. System Model

We consider a downlink RSMA scheme in a multi-user multi-cell VLC network, which comprises N_c attocells, where the i^{th} cell consists of N_l LED arrays and N_i single photo-detector (PD) users, $\forall i = 1, \dots, N_c$. The LED arrays in each attocell are connected to separate controllers in order to provide independent modulation. Moreover, band-limited backbone links are used for coordination purposes between the LED arrays of different attocells. It is assumed in this work that the coverage area of each attocell is determined by the union of the illumination of all LED arrays within the same attocell. Based on that, initially, the boundaries of the involved attocells are predetermined using a central processing unit, which also associates users to each attocell. Also, U_{ik} is used to denote for the intended message for the k^{th} user in the i^{th} attocell. In RSMA, the message U_{ik} is divided into a common part, U_{ik}^c , and a private part, U_{ik}^p . The common messages of all users in the i^{th} attocell are multiplexed and encoded into a single common stream, denoted by d_i^c , which is decoded by all i^{th} attocell users. On the other hand, U_{ik}^p is encoded as a private stream d_i^k to be decoded only by the k^{th} user. For the sake of simplicity and without loss of generality, the streams are assumed to be modulated using on-off keying (OOK) modulation scheme [28], and are assumed to be statistically independent with zero mean and unit variance.

In order to reduce interference, the linear precoder:

$$\mathbf{P}_i = [\mathbf{p}_i^c, \mathbf{p}_i^1, \mathbf{p}_i^2, \dots, \mathbf{p}_i^{N_i}] \in \mathbb{R}^{N_l \times (N_i + 1)}$$

is designed at each attocell and multiplied by the streams vector $\mathbf{d}_i = [d_i^c, d_i^1, \dots, d_i^{N_i}]^T$. In this work, the precoder matrices \mathbf{P}_i of each attocell are designed in coordinated manner, through exchanging the CSI of all UEs between all attocells. Then, a direct current (DC) bias vector:

$$\mathbf{I}_i^{\text{DC}} = I^{\text{DC}} \times \mathbf{1}_{N_l \times 1} \in \mathbb{R}^{N_l \times 1}$$

is added to ensure that the signals are positive at the LEDs input and also to set the illumination level in the room. To this end, the i^{th} attocell transmitted signal is written as follows

$$\mathbf{x}_i = \mathbf{P}_i \mathbf{d}_i + \mathbf{I}_i^{\text{DC}}, \quad \forall i = 1, \dots, N_c. \quad (1)$$

Based on the above, the received signal by the k^{th} user in the i^{th} attocell is the summation of the transmitted signals from all attocells, and can be expressed as

$$y_{ik} = (\mathbf{h}_{ik}^i)^T \mathbf{P}_i \mathbf{d}_i + \sum_{\substack{j=1 \\ j \neq i}}^{N_c} (\mathbf{h}_{ik}^j)^T \mathbf{P}_j \mathbf{d}_j + \sum_{j=1}^{N_c} (h_{ik}^j)^T \mathbf{I}_j^{\text{DC}} + n_{ik}, \quad (2)$$

where n_{ik} represents the additive white Gaussian noise (AWGN) with zero mean and variance

$$\sigma_{ik}^2 = \sigma_{ik,\text{sh}}^2 + \sigma_{ik,\text{th}}^2 \quad (3)$$

where $\sigma_{ik,\text{sh}}^2$ and $\sigma_{ik,\text{th}}^2$ denote the shot noise and thermal noise variances, respectively. Also, $\mathbf{h}_{ik}^j \in \mathbb{R}^{N_i \times 1}$ denotes the DC channel gain vector between the LED arrays of the j^{th} attocell and the k^{th} UE in the i^{th} attocell. To this effect and assuming that all utilized LED chips have the same specifications, the channel coefficient $h_{ik,n}^j$ between the n^{th} LED array of the j^{th} attocell and the k^{th} user in the i^{th} attocell can be expressed as follows [42]:

$$h_{ik,n}^j = \begin{cases} \frac{\zeta_n^j \zeta_k^i A_{ik} N_b}{(r_{ik,n}^j)^2} R_o(\varphi_{ik,n}^j) T_s(\phi_{ik}) g(\phi_{ik}) \cos(\phi_{ik}), & 0 \leq \phi_{ik} \leq \phi_c, \\ 0, & \text{otherwise,} \end{cases} \quad (4)$$

where ζ_n^j denotes the conversion factor of the n^{th} LED in the j^{th} attocell, ζ_k^i is the responsivity of the k^{th} UE's PD in the i^{th} attocell, A_{ik} represents the area of the PD, N_b is the number of LED chips per LED array, and $r_{ik,n}^j$ is the distance between the n^{th} LED array of the j^{th} attocell and the k^{th} UE in the i^{th} attocell. Moreover, $\varphi_{ik,n}^j$ is the transmission angle from the n^{th} LED in the j^{th} attocell to the k^{th} UE in the i^{th} attocell, ϕ_{ik} denotes the incident angle with respect to the receiver, and ϕ_c is the field of view (FoV) of the PD. Finally, $T_s(\phi_{ik})$ is the gain of the optical filter, and $g(\phi_{ik})$ is the gain of the optical concentrator, expressed as follows:

$$g(\phi_{ik}) = \begin{cases} \frac{n^2}{\sin^2(\phi_c)}, & 0 \leq \phi_{ik} \leq \phi_c, \\ 0, & \phi_{ik} > \phi_c, \end{cases} \quad (5)$$

where n is the refractive index and $R_o(\varphi_{ik,n}^j)$ is the Lambertian radiant intensity given by

$$R_o(\varphi_{ik,n}^j) = \frac{m+1}{2\pi} \left(\cos(\varphi_{ik,n}^j) \right)^m, \quad (6)$$

with m denoting the order of the Lambertian emission, written as

$$m = \frac{-\ln(2)}{\ln(\cos(\varphi_{1/2}))}, \quad (7)$$

where $\varphi_{1/2}$ represents the LED semi-angle at half power.

Note that the three first terms in (2) account for the useful transmitted information, IUI, and corresponding ICI, respectively. Due to the low mobility of indoor users in practical scenarios, we assume that the channel gains are static during the transmission. Moreover, we consider two scenarios, namely, perfect and imperfect CSI in order to design the precoding matrices \mathbf{P}_i , $\forall i = 1, \dots, N_c$. At the receiver, the effect of the involved DC signal is first eliminated from the received signal through an alternating current (AC) coupler. Then, the remaining part that carries the transmitted information is passed through a detector for signal decoding.

B. RSMA Data Decoding and Problem Formulation

In practical scenarios, the VLC wireless channel may experience uncertainty, mainly due to the uplink and downlink noises, as well as the mobility of users in the indoor environment. To this effect and in order to align our work with real-environment conditions, we characterize the incurred CSI uncertainties by adopting the random error model [43]. Therefore, the estimated channel coefficients can be represented by

$$\hat{\mathbf{h}}_{ik}^j = \mathbf{h}_{ik}^j + \mathbf{e}_{ik}^j, \quad (8)$$

where $\hat{\mathbf{h}}_{ik}^j$ is the channel estimate, and \mathbf{e}_{ik}^j is the estimation error vector with each of its component drawn from a Gaussian distribution with zero mean and variance σ_e^2 . In this work, we adopt the minimum mean squared error (MMSE) linear precoding. The reason is that MMSE-based precoding enjoys high performance, especially at low SNR regimes, and is relatively less restrictive in terms of required number of transmitting LEDs, compared to other linear precoding techniques. Using RSMA, the k^{th} user in the i^{th} attocell has to firstly decode the common stream d_i^c . Hence, the average of the MSE estimate of the common message can be expressed as follows:

$$\bar{E}_{ik}^c = \mathbb{E}_{\mathbf{e}_i} [E_{ik}^c] = (\alpha_{ik}^c)^2 \bar{\rho}_{ik}^c - 2\alpha_{ik}^c (\mathbf{h}_{ik}^i)^T \mathbf{p}_i^c + 1, \quad (9)$$

given that

$$E_{ik}^c = \mathbb{E} \left(\left\| \hat{d}_{ik}^c - d_i^c \right\|^2 \right), \quad (10)$$

where E_{ik}^c denotes the instantaneous common message MSE given that $\hat{d}_{ik}^c = \alpha_{ik}^c \tilde{y}_{ik}$ is the estimate of the stream d_i^c at the k^{th} user. Also, \tilde{y}_{ik} denotes the received AC signal and α_{ik}^c denotes the receive filter of the stream d_i^c at the k^{th} user. Furthermore, $\bar{\rho}_{ik}^c$ is given by

$$\bar{\rho}_{ik}^c = \sum_{j=1}^{N_c} \left\| \left(\mathbf{h}_{ik}^j \right)^T \mathbf{P}_j \right\|^2 + \sigma_e^2 \text{Trac}(\mathbf{P}_j^T \mathbf{P}_j) + \sigma_{ik}^2. \quad (11)$$

In what follows, we first recall that the common stream of the i^{th} attocell is decoded by all users within the same cell. Therefore, in order to guarantee a successful decoding of the common stream by all users, we aim to evaluate the worst case scenario for which the common stream MSE is chosen as the maximum value among all users as follows:

$$E_i^c = \max_{k \in \{1, 2, \dots, N_i\}} \bar{E}_{ik}^c. \quad (12)$$

After successful decoding of d_i^c , the effect of the common message is removed from \tilde{y}_{ik} by utilizing SIC. Then, the k^{th} UE in the i^{th} attocell decodes its corresponding private stream d_i^k assuming all remaining streams as a noise. Hence, the average of the MSE estimate of the private stream is given by

$$\bar{E}_i^k = \mathbb{E}_{\mathbf{e}_i} [E_i^k] = (\alpha_i^k)^2 \bar{\rho}_i^k - 2\alpha_i^k (\mathbf{h}_{ik}^i)^T \mathbf{p}_i^k + 1, \quad (13)$$

given that

$$E_i^k = \mathbb{E} \left(\left\| \hat{d}_i^k - d_i^k \right\|^2 \right), \quad (14)$$

where E_i^k is the instantaneous private message MSE given that

$$\hat{d}_i^k = \alpha_i^k \left(\tilde{y}_{ik} - (\mathbf{h}_{ik}^i)^T \mathbf{p}_i^c d_i^c \right), \quad (15)$$

which denotes for the estimate of the stream d_i^k and α_i^k denotes the receive filter for the stream d_i^k . Also, $\bar{\rho}_i^k$ is expressed as follows:

$$\begin{aligned} \bar{\rho}_i^k &= \sum_{\ell=1}^{N_i} \left| (\mathbf{h}_{ik}^i)^T \mathbf{p}_i^\ell \right|^2 + \sigma_e^2 \|\mathbf{p}_i^\ell\|^2 \\ &+ \sum_{j=1, j \neq i}^{N_c} \left\| (\mathbf{h}_{ik}^j)^T \mathbf{P}_j \right\|^2 + \sigma_e^2 \text{Trac}(\mathbf{P}_j^T \mathbf{P}_j) + \sigma_{ik}^2. \end{aligned} \quad (16)$$

Similar to [28], we design the precoders for the common and private streams by formulating a SMSE minimization problem while taking into account imperfect CSI at the transmitters and assuming that the attocells coordinate with each other. Hence, utilizing the stochastic error model in (8), we aim at optimizing the average performance over the error vector, which guarantees a system performance averaged over multiple error realizations. The CB-based RSMA optimization problem can be formulated as

$$\min_{\mathbf{P}_i, E_i^c, \alpha_i^k, \alpha_{ik}^c} \mathbb{E}_{\mathbf{e}_i} (\text{SMSE}) \quad (\text{P1})$$

$$\text{s.t. } \bar{E}_{ik}^c \leq E_i^c, \quad \forall k, \forall i \quad (\text{P1.a})$$

$$L_1(\mathbf{p}_i^\ell) \leq \min(I^{\text{DC}} - I_{\min}, I_{\max} - I^{\text{DC}}) \mathbf{1}_{N_i \times 1}, \quad \forall \ell \quad (\text{P1.b})$$

where

$$\text{SMSE} = \sum_{i=1}^{N_c} E_i^c + \sum_{i=1}^{N_c} \sum_{k=1}^{N_i} \bar{E}_i^k. \quad (18)$$

In (P1), \mathbf{p}_i^ℓ denotes for the ℓ^{th} row of the matrix \mathbf{P}_i . Constraint (P1.b) accounts for the optical power constraints at each LED. It is worth highlighting that (P1) is different from the proposed formulation problem of RSMA-based multi-cell VLC in [38]. There, all attocells were considered as a single large cell to jointly serve all users in the network. However, in the currently proposed optimization framework we consider the design of the common/private precoders of different attocells in a coordinated manner, with the aim to reduce experienced interference and complexity by combining CB and RSMA. It is worth noting that, (P1) is non-convex in terms of all variables. Hence, its solution is non-trivial and rather difficult. In the next section, we propose an effective suboptimal solution to (P1) using an AO-based method.

III. PROPOSED SOLUTION

In order to solve the joint optimization problem (P1), we utilize a low-complexity sub-optimal iterative algorithm, based on the AO, where the algorithm iterates between updating the receive filters and precoders until convergence. Assuming that the precoding matrices \mathbf{P}_i and common MSE variables E_i^c are

Algorithm 1: AO Algorithm.

- 1: Initialize $t \leftarrow 0$, $\mathbf{P}_i^{[t]} E_i^{c[t]}, \forall i$
 - 2: **repeat**
 - 3: $t \leftarrow t + 1$; $\mathbf{P}_i^{[t-1]} \leftarrow \mathbf{P}_i$
 - 4: Update the MMSE receive filter coefficients
 $\alpha_{ik}^c \leftarrow \alpha_{ik}^c(\mathbf{P}_i^{[t-1]})$ and $\alpha_i^k \leftarrow \alpha_i^k(\mathbf{P}_i^{[t-1]})$
 - 5: Solve (P1) for optimized $(\alpha_{ik}^c, \alpha_i^k)$, then update
 (\mathbf{P}_i, E_i^c)
 - 6: **until** $|\text{SMSE}^{[t]} - \text{SMSE}^{[t-1]}| \leq \delta$ or N_{\max} is reached.
-

fixed, a closed-form solution for the optimum receive filter coefficients for the common and the private messages can be obtained as

$$(\alpha_{ik}^c)^* = \frac{(\mathbf{h}_{ik}^i)^T \mathbf{p}_i^c}{\bar{\rho}_{ik}^c}, \quad (19)$$

and

$$(\alpha_i^k)^* = \frac{(\mathbf{h}_{ik}^i)^T \mathbf{p}_i^k}{\bar{\rho}_i^k}, \quad (20)$$

respectively. On the contrary, by fixing the receive filter coefficients values, the joint optimization problem of the precoders and common MSEs becomes a quadratically constrained quadratic programming (QCCP) problem. As a result, it can be solved using the MOSEK solver of CVX tool [44]. Subsequently, a sub-optimal solution for (P1) is obtained through AO, as illustrated in Algorithm 1. At the t^{th} iteration of Algorithm 1, the receive filter coefficients are updated using the precoder values of all attocells, obtained in the $(t-1)^{\text{th}}$ iteration using (19) and (20). Then, the precoder values and the common MSEs are updated by solving (P1) with the optimized receive filter coefficients. Finally, this procedure is iteratively repeated until convergence, i.e., difference of the SMSEs is below a predefined threshold δ , or the maximum number of iterations N_{\max} is reached.

A. Complexity Analysis of Algorithm 1

In Algorithm 1, the complexity of solving problem (P1) resides mainly in the complexity of solving the QCCP of the precoding vectors for fixed receive filter coefficients. It is worth noting that for fixed receive filters, problem (P1) comprises

$$Y_1 = N_\ell N_c + \sum_{i=1}^{N_c} N_i \quad (21)$$

constraints and

$$Y_2 = N_c(N_\ell + 1) + N_\ell \sum_{i=1}^{N_c} N_i \quad (22)$$

scalar variables. Thus, if the interior-point method is used, the worst-case computational complexity of solving the QCCP is

$$\mathcal{O} \left((Y_1 Y_2^2 + Y_2^3) \sqrt{Y_1} \log(1/\delta) \right)$$

for a given solution accuracy δ [45], [46].

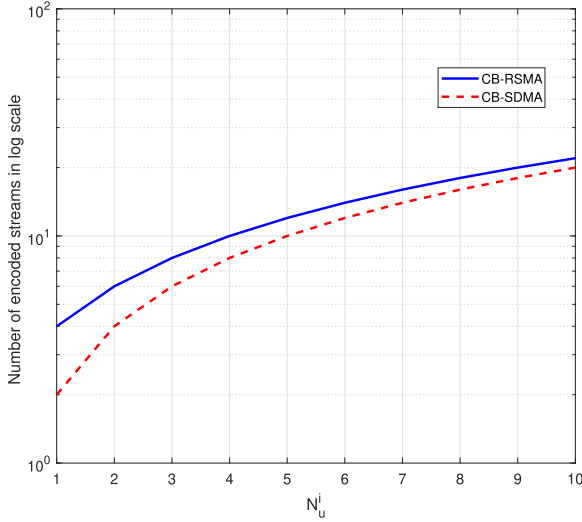


Fig. 1. Complexity of the CB-RSMA and CB-SDMA schemes in terms of the overall number of streams in the network.

B. Complexity of RSMA in Multi-Cell Configurations

In the proposed framework, although RSMA scheme is more efficient and outperforms SDMA for different network loads and users deployments, it comes at the expense of slightly increased encoder complexity. That is for RSMA in multi-cell setup, a total of $\sum_{i=1}^{N_c} N_i + 1$ messages need to be encoded in the network, whilst $\sum_{i=1}^{N_c} N_i$ messages are encoded in case of using SDMA. Fig. 1 illustrates the overall number of streams for both RSMA and SDMA in two cells network as a function of the number of user in each cell N_i . It is clear from the figure that CB-RSMA has a slightly higher number of encoded streams compared to CB-SDMA.

Besides the slightly increased encoder complexity, using RSMA would also increase the decoder complexity, which is attributed to the need for one SIC operation at each user in order to decode the common stream and subtract it to enhance the detection of the private stream. In contrast, SDMA scheme does not require any SIC operation at the receiver side and each user decodes its intended stream directly assuming any interference of other users' messages as noise. Additionally, in practice, the uncertainty in the CSI is inevitable in multi-cell RSMA VLC networks, which may lead to a scenario that the interference of the common streams can not be completely removed during the SIC operation at the receiver side. Consequently, this makes RSMA subjected to error propagation leading to a degradation in the error rate performance. On the contrary, as SDMA users do not require any SIC layer at the receive side, error propagation does not occur as in RSMA, hence, SDMA is less susceptible to error rate degradation. However, in overloaded setups, where the number of users in each cell exceeds the number of available LED arrays, SDMA users suffer from high interference from other users' messages due to the reduced spatial multiplexing gain. Thus, RSMA enjoys better error rate performance in overloaded setups, thanks to its ability to handle the network's interference through messages splitting.

C. Performance Metrics

Here, we use the SE and EE as key performance indicators to compare the performance of RSMA and the recent multiple access scheme SDMA¹ when combined with CB, for different users scenarios. Based on the well-known Shannon's capacity theorem, the achievable data rates for decoding the common/private messages are written as [38]²

$$R_{ik}^c = B \log_2(1 + \gamma_{ik}^c), \quad (23)$$

and

$$R_i^k = B \log_2(1 + \gamma_i^k), \quad \forall i, \forall k, \quad (24)$$

respectively, where B denotes the bandwidth. Also, γ_{ik}^c and γ_i^k are the corresponding received SINRs of the common and private streams at the k^{th} user of the i^{th} attocell, and are expressed, respectively as

$$\gamma_{ik}^c = \frac{\left((\mathbf{h}_{ik}^i)^T \mathbf{p}_i^c \right)^2 + \sigma_e^2 \|\mathbf{p}_i^c\|^2}{\bar{\rho}_i^k} \quad (25)$$

and

$$\gamma_i^k = \frac{\left((\mathbf{h}_{ik}^i)^T \mathbf{p}_i^k \right)^2 + \sigma_e^2 \|\mathbf{p}_i^k\|^2}{\bar{\rho}_i^k - \left| (\mathbf{h}_{ik}^i)^T \mathbf{p}_i^k \right|^2 - \sigma_e^2 \|\mathbf{p}_i^k\|^2}. \quad (26)$$

To successfully decode the common stream at all users, the common rate in attocell i should satisfy the following condition

$$R_i^c = \min(R_{i1}^c, R_{i2}^c, \dots, R_{iN_i}^c). \quad (27)$$

Consequently, the corresponding system SE and EE are defined as [47], [48]

$$\eta_{SE} = \frac{1}{B} \sum_{i=1}^{N_c} \left[R_i^c + \sum_{k=1}^{N_i} R_i^k \right] \quad (28)$$

and

$$\eta_{EE} = \frac{\eta_{SE}}{BP_T}, \quad (29)$$

respectively, where P_T is the total power consumption of the system [49] given as follows:

$$P_T = N_b^2 \sum_{i=1}^{N_c} \mathbb{E}(\|\mathbf{x}_i\|^2) \quad (30)$$

It would be mentioned that for the case of perfect CSI, all derived equations and optimization problem (P1) are still valid by setting $\sigma_e^2 = 0$.

¹ It has been demonstrated in [31], [34] that RSMA has reduced complexity and superior performance compared to NOMA in MIMO systems, which is attributed to the latter's inefficient use of spatial dimensions. Hence, the comparison between CB-based NOMA and CB-based RSMA is not carried-out in our study.

² It is noted here that Shannon's capacity equations can still be used for VLC systems if the transmitted signal is frequency-upshifted. Wherein, the real-valued baseband transmission signal model for VLC can be converted into a complex-valued baseband channel by applying a frequency-upshift to an intermediate frequency (IF), which has a slightly higher center frequency than half the bandwidth of the transmitted signal before applying the bias current.

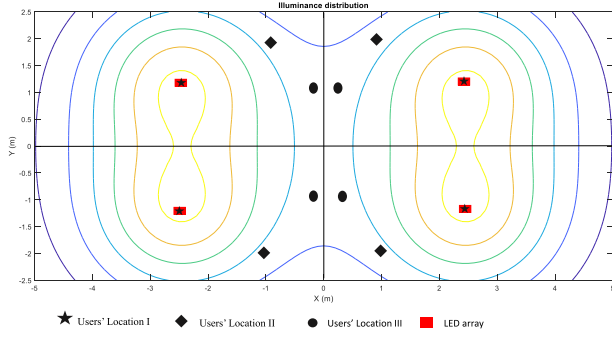


Fig. 2. Multi-cell illuminance distribution of the considered setup.

 TABLE I
SIMULATION PARAMETERS

Parameter	Symbol	Value
Number of LED chips per array	N_b	3600 (60×60)
LED semi-angle at half power	$\varphi_{1/2}$	70°
PD area	A	1 cm^2
Refractive index of PD	n	1.5
Gain of optical filter	$T_s(\phi)$	1
FoV of PD	ϕ_c	60°
Maximum allowable current	I_{\max}	600 mA
Minimum allowable current	I_{\min}	400 mA
DC current	I^{DC}	500 mA
Bandwidth	B	20 MHz

 TABLE II
USERS' LOCATIONS ($N_i = 2$)

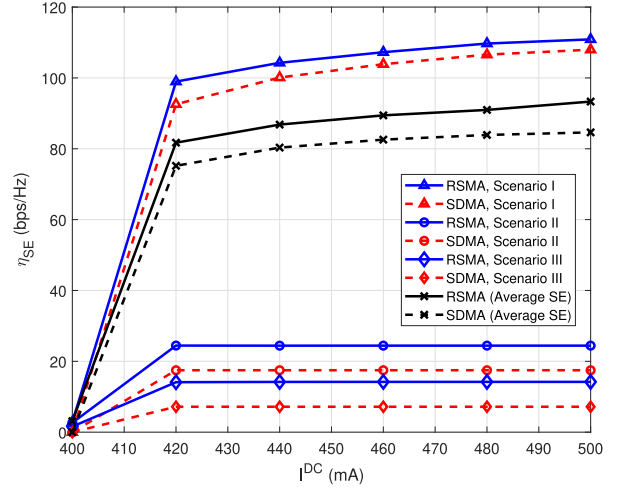
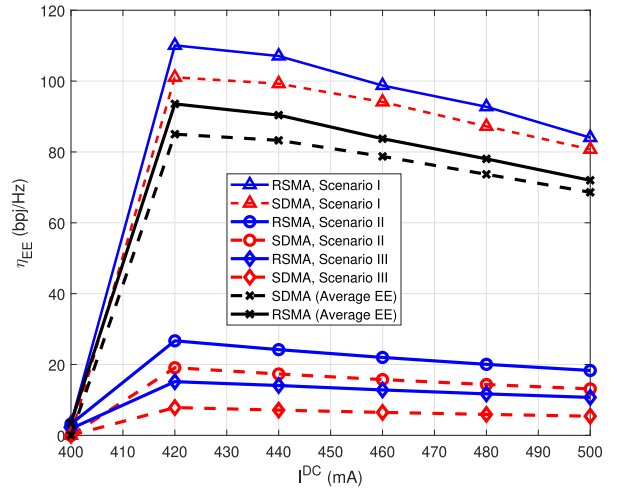
	Cell 1	Cell 2
Scenario I	User 1: [2.5,1.25,0.85] User 2: [2.5,-1.25,0.85]	User 3: [-2.5,1.25,0.85] User 4: [-2.5,-1.25,0.85]
Scenario II	User 1: [1,2,0.85] User 2: [1,-2,0.85]	User 3: [-1,2,0.85] User 4: [-1,-2,0.85]
Scenario III	User 1: [0.25,1.25,0.85] User 2: [0.25,-1.25,0.85]	User 3: [-0.25,1.25,0.85] User 4: [-0.25,-1.25,0.85]

IV. NUMERICAL RESULTS

This section capitalizes on the offered results in the previous sections to thoroughly quantify the achievable performance of the considered multi-cell multi-user VLC system. To this end, we demonstrate different scenarios for integrating CB-based RSMA in multi-user multi-cell VLC systems. The corresponding performance in each case is evaluated in terms of the SE and EE, as expressed in (28)–(29). In addition, the achievable performance for each case is compared to that of the corresponding CB-based SDMA scheme. We assume an indoor environment with dimensions $10 \times 5 \times 3 \text{ m}^3$, whilst $N_c = 2$, $N_i = 2$, and $N_i = 2$, $\forall i = 1, \dots, N_c$. Also, the illuminance distribution in the considered cells is shown in Fig. 2. Without loss of generality, we further assume that $\zeta = 1 \text{ W/A}$ and $\zeta = 1 \text{ A/W}$. Additionally, the remaining parameters, without loss of generality, are selected according to [50] and as listed in Table I. Different scenarios have been defined with different locations for users and LED arrays which are presented in Tables II and III, respectively. For convenience, the considered scenarios and the illuminance distribution for the two attocells are illustrated in Fig. 2.

 TABLE III
LED ARRAYS' LOCATIONS

Cell 1	Cell 2
LED array 1: [2.5,1.25,3]	LED array 3: [-2.5,1.25,3]
LED array 2: [2.5,-1.25,3]	LED array 4: [-2.5,-1.25,3]


 Fig. 3. SE vs. DC bias in case of perfect CSI (different scenarios, $N_i = 2$).

 Fig. 4. EE vs. DC bias in case of perfect CSI (different scenarios, $N_i = 2$).

In Fig. 3 we compare the achievable SE performance of both CB-based RSMA and CB-based SDMA schemes as functions of the DC bias at the LEDs input, given the scenarios I to III. Also, we plot their averaged SE over randomized locations scenarios. It is noted that, as I^{DC} increases, SE enhances rapidly up to $I^{\text{DC}} = 420 \text{ mA}$, and then slowly reaches its maximum value at $I^{\text{DC}} = 500 \text{ mA}$. However, for scenarios where users experience high ICI, the SE saturates rapidly. Finally, it is shown that CB-based RSMA outperforms CB-based SDMA in terms of average achievable SE due to its interference reduction capabilities through messages splitting that allows each user to decode part of the interference and treat the remaining part as noise. Additionally, Fig. 4 illustrates the corresponding EE as

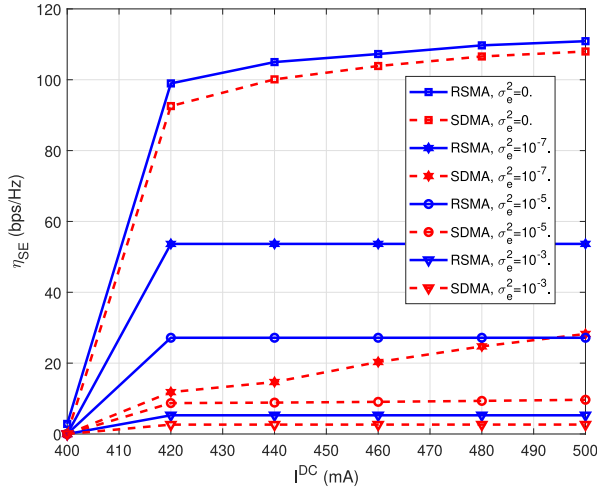


Fig. 5. Impact of the CSI uncertainty on SE performance (scenario I, $N_i = 2$).

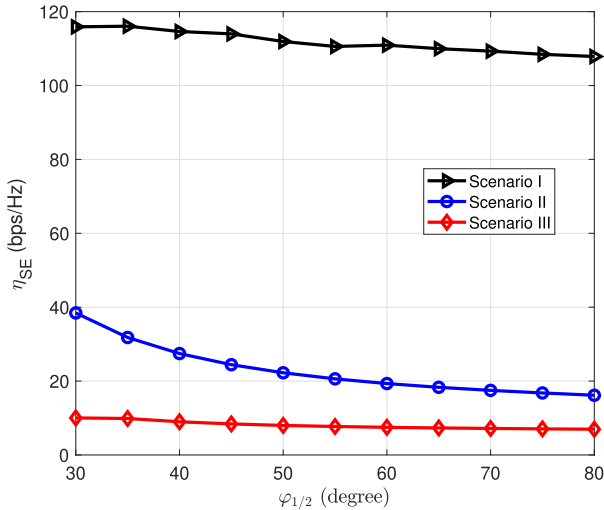


Fig. 6. SE vs. $\varphi_{1/2}$ (CB RSMA, different scenarios).

a function of the DC bias. For all scenarios, it is shown that as I^{DC} increases up-to 420 mA, the EE is enhanced due to the achieved high SE compared to power consumption. Then, as the DC current exceeds 420 mA, the EE begins to decrease, since more power is consumed in this region, but a small additional SE gain is achieved. As in Fig. 3, CB-based RSMA provides better EE performance compared to CB-based SDMA in all scenarios.

In order to demonstrate the impact of the involved channel uncertainty, we investigate the SE performance of the proposed scheme for different values of the parameter σ_e^2 in Fig. 5. We notice that as σ_e^2 grows, even with small values, the SE performance is significantly degraded. Nevertheless, the proposed CB-based RSMA demonstrates higher robustness to channel uncertainty compared to CB-based SDMA. For instance, the percentage drop in the SE for CB-based RSMA is about 51.6% while it reaches 73.85% for CB-based SDMA, given that $\sigma_e^2 = 10^{-7}$. Hence, it becomes evident that channel estimation errors should not be neglected in practical communication scenarios. In Fig. 6,

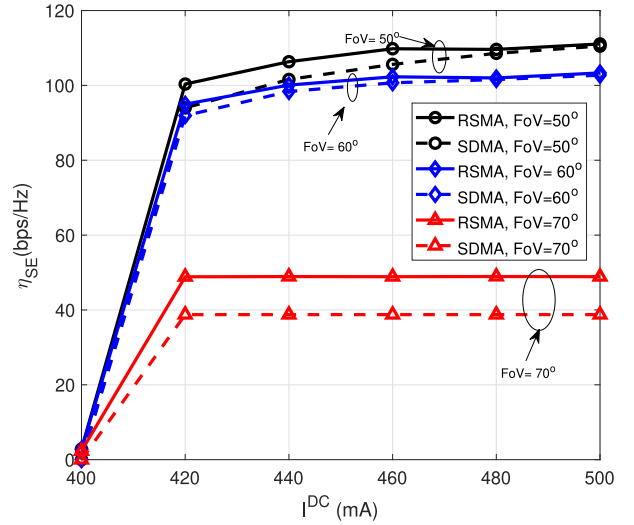


Fig. 7. SE vs. DC bias for perfect CSI (scenario I, different FoVs).

we evaluate the impact of the LED semi-angle at half power, $\varphi_{1/2}$, on the SE of the CB-based RSMA scheme. The best SE performance is achieved for low $\varphi_{1/2}$ values as a small $\varphi_{1/2}$ (close to 0°) leads to an increased Lambertian radiant intensity, which in turn improves the quality of the communication channel, while reducing its correlation. In contrast, a high $\varphi_{1/2}$ (close to 90°) degrades the quality of the channel and hence decreases the corresponding SE. The effect of PDs' FoV is quantified in Fig. 7, where it is observed that as the FoV increases from 50° to 60°, the corresponding SE degrades slightly. However, when the FoV is set at 70°, the degradation becomes more significant i.e. close to 60%. On the one hand, using PDs with high FoV angle would increase the collective area, but causes a significant ICI that degrades the communication quality. On the other hand, PDs with a small FoV have low-range collective areas but they generate a small ICI that significantly improves the achievable SE.

Subsequently, in Fig. 8 we study the convergence in terms of SMSE, of the AO algorithm for the cases of perfect and imperfect CSI, when the DC bias is 500 mA. For perfect CSI, the algorithm converges to the best performance after approximately 10 iterations in all scenarios. Conversely, it converges in less than 4 iterations when the system experiences the detrimental effects of CSI uncertainty. Indeed, CSI uncertainty introduces an additional noise component, as seen in (11) and (16), which limits the optimization search space, and hence provides a faster result. In any case, it is noted that imperfect CSI provides highly degraded performances compared to perfect CSI.

Differently from the previous results, Fig. 9 demonstrates the SE performance of the CB-based RSMA and CB-based SDMA versus the DC bias for overloaded regime, i.e., the number of users N_i is larger than the available LEDs in each attocell N_l , where the number of users per cell is fixed to $N_i = 3$ rather than $N_i = 2$. The considered scenarios are defined as follows: Scenario I and II are identical to the ones presented in Table II, to which we added two new users at different locations, namely User 5 [1,1,0.85] and User 6 [-1,-1,0.85] for Scenario I, and

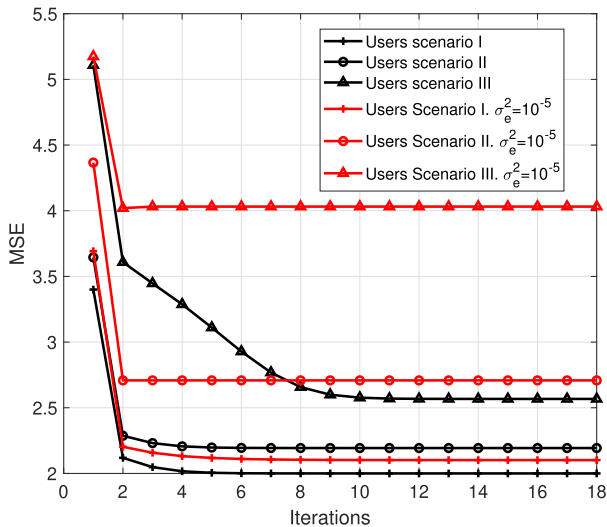


Fig. 8. AO algorithm convergence ($I^{DC} = 500 \text{ mA}$, different scenarios).

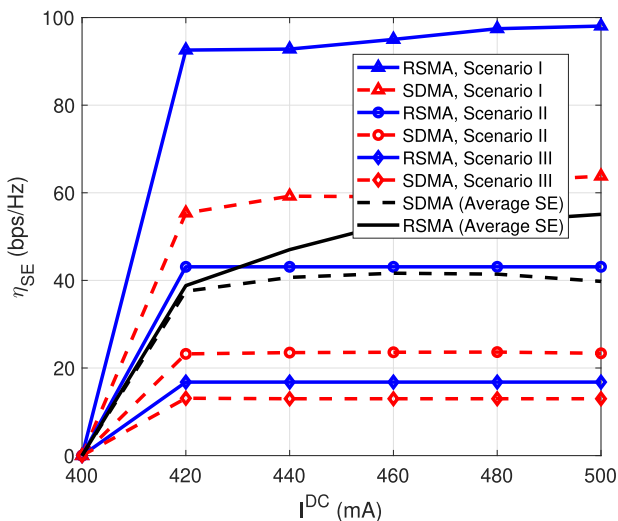


Fig. 9. SE vs. DC bias ($N_i = 3$, different scenarios).

User 5 $[3, 3, 0.85]$ and User 6 $[-3, -3, 0.85]$ for Scenario II. For Scenario III, we considered the following users locations: User 1 $[1, 1, 0.85]$, User 2 $[1, -1, 0.85]$, User 3 $[0.5, 0.5, 0.85]$, User 4 $[-1, 1, 0.85]$, User 5 $[-1, -1, 0.85]$, and User 6 $[-0.5, -0.5, 0.85]$. Similarly to Fig. 3, the achievable SE appears to improve quickly up to $I^{DC} = 420 \text{ mA}$, and then grows slower to its maximum at $I^{DC} = 500 \text{ mA}$. Hence, N_i has no impact on the best I^{DC} values. Moreover, we notice that the achievable SE performance for $N_i = 3$ is overall below that of $N_i = 2$ (Fig. 3), and the performance gap between the two schemes becomes larger as the number of users exceeds the available LEDs in each attocell. Indeed, as the number of users to be served increases, coordination becomes more complex and less-efficient in the presence of higher incurred ICI. Finally, CB-based RSMA turns out to be superior to CB-based SDMA in all scenarios, thus validating its usefulness for higher-scale systems.

V. CONCLUSION

In this paper we investigated multiple access for multi-cell MISO VLC systems. In order to tackle the high ICI issue for cell-edge users, coordination between VLC cells is required. And even though joint transmission multiple access achieves the best performance, it is not very practical due to its increased communication costs. Therefore, we proposed CB-based RSMA scheme, that brings extra benefits in terms of interference mitigation and complexity. Through extensive computer simulations, we compared the efficiency of our proposed CB-based RSMA method with the conventional CB-based SDMA, in terms of SE, and EE. Moreover, the impact of several parameters on the overall system performance has been investigated, allowing to draw the following insights: 1) Imperfect CSI significantly degrades the CB-based RSMA performances, however, our proposed scheme was more robust to the imperfect CSI compared to CB-based SDMA; 2) DC bias value has to be set to maximum in order to achieve the best SE performance, while kept at the critical value of 420 mA for the best EE performance, which is independent of the number of users in the system; 3) low values for the LED semi-angle at half power and the FoV achieve the best SE performances. The offered results and the developed insights are anticipated to be particularly useful in the successful design and deployment of future multi-user multi-cell VLC systems.

REFERENCES

- [1] A. R. Ndjiongue, T. M. N. Ngatched, O. A. Dobre, and A. G. Armada, "VLC-based networking: Feasibility and challenges," *IEEE Netw.*, vol. 34, no. 4, pp. 158–165, Jul./Aug. 2020.
- [2] S. Feng, R. Zhang, W. Xu, and L. Hanzo, "Multiple access design for ultra-dense VLC networks: Orthogonal vs non-orthogonal," *IEEE Trans. Commun.*, vol. 67, no. 3, pp. 2218–2232, Mar. 2019.
- [3] A. M. Vegni and M. Biagi, "Optimal LED placement in indoor VLC networks," *Opt. Exp.*, vol. 27, no. 6, pp. 8504–8519, Mar. 2019. [Online]. Available: <http://opg.optica.org/oe/abstract.cfm?URI=oe-27-6-8504>
- [4] N. E. Mahfouz, H. A. Fayed, A. Abd El Aziz, and M. H. Aly, "Improved light uniformity and SNR employing new LED distribution pattern for indoor applications in VLC system," *Opt. Quantum Electron.*, vol. 50, no. 9, pp. 1–18, 2018.
- [5] F. Ahmed, A. A. Dowhuszko, and O. Tirkkonen, "Self-organizing algorithms for interference coordination in small cell networks," *IEEE Trans. Veh. Technol.*, vol. 66, no. 9, pp. 8333–8346, Sep. 2017.
- [6] R. Bai, H. Tian, B. Fan, and S. Liang, "Coordinated transmission based interference mitigation in VLC network," in *Proc. IEEE 82nd Veh. Technol. Conf.*, 2015, pp. 1–5.
- [7] B. G. Guzmán, A. A. Dowhuszko, V. P. G. Jiménez, and A. I. Pérez-Neira, "Resource allocation for cooperative transmission in optical wireless cellular networks with illumination requirements," *IEEE Trans. Commun.*, vol. 68, no. 10, pp. 6440–6455, Oct. 2020.
- [8] J. Deng, X. Jin, X. Ma, M. Jin, C. Gong, and Z. Xu, "Graph-based scheduling for cooperative transmission in indoor VLC systems," in *Proc. IEEE Int. Conf. Commun. Workshops*, 2019, pp. 1–6.
- [9] S. Aboagye, T. M. N. Ngatched, O. A. Dobre, and A. G. Armada, "Energy efficient subchannel and power allocation in cooperative VLC systems," *IEEE Commun. Lett.*, vol. 25, no. 6, pp. 1935–1939, Jun. 2021.
- [10] M. Obeed, A. M. Salhab, S. A. Zummo, and M. Alouini, "Joint power allocation and cell formation for energy-efficient VLC networks," in *Proc. IEEE Int. Conf. Commun.*, 2018, pp. 1–6.
- [11] K. Zhou, C. Gong, and Z. Xu, "Color planning and intercell interference coordination for multicolor visible light communication networks," *J. Lightw. Technol.*, vol. 35, no. 22, pp. 4980–4993, Oct. 2017.
- [12] S. A. Naser and P. C. Sofotasios, "Generalization of space-time block coded-spatial modulation for high data rate VLC systems," in *Proc. 3rd Int. Conf. Adv. Commun. Technol. Netw.*, 2020, pp. 1–5.

- [13] S. Naser *et al.*, "Toward federated-learning-enabled visible light communication in 6G systems," *IEEE Wireless Commun.*, vol. 29, no. 1, pp. 48–56, Feb. 2022.
- [14] M. Elamassie, L. Bariah, M. Uysal, S. Muhaidat, and P. C. Sofotasios, "Capacity analysis of NOMA-enabled underwater VLC networks," *IEEE Access*, vol. 9, pp. 153 305–153315, 2021.
- [15] A. Al Hammadi, P. C. Sofotasios, S. Muhaidat, M. Al-Qutayri, and H. Elgala, "Non-orthogonal multiple access for hybrid VLC-RF networks with imperfect channel state information," *IEEE Trans. Veh. Technol.*, vol. 70, no. 1, pp. 398–411, Jan. 2021.
- [16] S. Naser, L. Bariah, S. Muhaidat, M. Al-Qutayri, and P. C. Sofotasios, "An effective spatial modulation based scheme for indoor VLC systems," *IEEE Photon. J.*, vol. 14, no. 1, Feb. 2022, Art. no. 7314111.
- [17] L. Bariah, M. Elamassie, S. Muhaidat, P. C. Sofotasios, and M. Uysal, "Non-orthogonal multiple access-based underwater VLC systems in the presence of turbulence," *IEEE Photon. J.*, vol. 14, no. 1, Feb. 2022, Art. no. 7308707.
- [18] S. Naser, L. Bariah, S. Muhaidat, M. Al-Qutayri, M. Uysal, and P. C. Sofotasios, "Space-time block coded spatial modulation for indoor visible light communications," *IEEE Photon. J.*, vol. 14, no. 1, Feb. 2022, Art. no. 7303111.
- [19] J. Lian and M. Brandt-Pearce, "Multiuser visible light communication systems using OFDMA," *J. Lightw. Technol.*, vol. 38, no. 21, pp. 6015–6023, 2020.
- [20] B. Genovés Guzmán, A. A. Dowhuszko, V. P. Gil Jiménez, and A. I. Pérez-Neira, "Robust cooperative multicarrier transmission scheme for optical wireless cellular networks," *IEEE Photon. Technol. Lett.*, vol. 30, no. 2, pp. 197–200, Jan. 2018.
- [21] S.-Y. Jung, D.-H. Kwon, S.-H. Yang, and S.-K. Han, "Inter-cell interference mitigation in multi-cellular visible light communications," *Opt. Exp.*, vol. 24, no. 8, pp. 8512–8526, Apr. 2016.
- [22] S.-Y. Jung, D. Kwon, S.-H. Yang, and S.-K. Han, "Reduction of inter-cell interference in asynchronous multi-cellular VLC by using OFDMA-based cell partitioning," in *Proc. 18th Int. Conf. Transparent Opt. Nets.*, 2016, pp. 1–4.
- [23] C. Chen, W. Zhong, H. Yang, S. Zhang, and P. Du, "Reduction of SINR fluctuation in indoor multi-cell VLC systems using optimized angle diversity receiver," *J. Lightw. Technol.*, vol. 36, no. 17, pp. 3603–3610, May 2018.
- [24] K. Ying, H. Qian, R. J. Baxley, and S. Yao, "Joint optimization of precoder and equalizer in MIMO VLC systems," *IEEE J. Sel. Areas Commun.*, vol. 33, no. 9, pp. 1949–1958, Sep. 2015.
- [25] M. S. Demir, H. B. Eldeeb, and M. Uysal, "CoMP-based dynamic handover for vehicular VLC networks," *IEEE Commun. Lett.*, vol. 24, no. 9, pp. 2024–2028, Sep. 2020.
- [26] T. V. Pham and A. T. Pham, "Coordination/cooperation strategies and optimal zero-forcing precoding design for multi-user multi-cell VLC networks," *IEEE Trans. Commun.*, vol. 67, no. 6, pp. 4240–4251, Jun. 2019.
- [27] H. Yang, C. Chen, W. Zhong, and A. Alphones, "Joint precoder and equalizer design for multi-user multi-cell MIMO VLC systems," *IEEE Trans. Veh. Technol.*, vol. 67, no. 12, pp. 11 354–11 364, Dec. 2018.
- [28] H. Ma, A. Mostafa, L. Lampe, and S. Hranilovic, "Coordinated beamforming for downlink visible light communication networks," *IEEE Trans. Commun.*, vol. 66, no. 8, pp. 3571–3582, Aug. 2018.
- [29] Y. Mao, O. Dizdar, B. Clerckx, R. Schober, P. Popovski, and H. V. Poor, "Rate-splitting multiple access: Fundamentals, survey, and future research trends," 2022. [Online]. Available: <https://arxiv.org/abs/2201.03192>
- [30] B. Clerckx, H. Joudeh, C. Hao, M. Dai, and B. Rassouli, "Rate splitting for MIMO wireless networks: A promising PHY-layer strategy for LTE evolution," *IEEE Commun. Mag.*, vol. 54, no. 5, pp. 98–105, May 2016.
- [31] Y. Mao, B. Clerckx, and V. Li, "Rate-splitting multiple access for downlink communication systems: Bridging, generalizing, and outperforming SDMA and NOMA," *EURASIP J. Wireless Commun. Netw.*, vol. 2018, no. 1, pp. 1–54, May 2018.
- [32] O. Dizdar, Y. Mao, W. Han, and B. Clerckx, "Rate-splitting multiple access: A new frontier for the PHY layer of 6G," in *Proc. IEEE 92nd Veh. Technol. Conf.*, 2020, pp. 1–7.
- [33] L. Yin and B. Clerckx, "Rate-splitting multiple access for multigroup multicast and multibeam satellite systems," *IEEE Trans. Commun.*, vol. 69, no. 2, pp. 976–990, Feb. 2020.
- [34] Y. Mao and B. Clerckx, "Beyond dirty paper coding for multi-antenna broadcast channel with partial CSIT: A rate-splitting approach," *IEEE Trans. Commun.*, vol. 68, no. 11, pp. 6775–6791, Nov. 2020.
- [35] W. Jaafar, S. Naser, S. Muhaidat, P. C. Sofotasios, and H. Yanikomeroglu, "Multiple access in aerial networks: From orthogonal and non-orthogonal to rate-splitting," *IEEE Open J. Veh. Technol.*, vol. 1, pp. 372–392, 2020.
- [36] W. Jaafar, S. Naser, S. Muhaidat, P. C. Sofotasios, and H. Yanikomeroglu, "On the downlink performance of RSMA-based UAV communications," *IEEE Trans. Veh. Technol.*, vol. 69, no. 12, pp. 16 258–16 263, Dec. 2020.
- [37] S. Naser *et al.*, "Rate-splitting multiple access: Unifying NOMA and SDMA in MISO VLC channels," *IEEE Open J. Veh. Technol.*, vol. 1, pp. 393–413, Oct. 2020.
- [38] S. Tao, H. Yu, Q. Li, Y. Tang, and D. Zhang, "One-layer rate-splitting multiple access with benefits over power-domain NOMA in indoor multi-cell visible light communication networks," in *Proc. IEEE Int. Conf. Commun. Workshops*, 2020, pp. 1–7.
- [39] S. Ma *et al.*, "Robust beamforming design for rate splitting multiple access-aided MISO visible light communications," 2021, *arXiv:2108.07014*.
- [40] F. Xing, S. He, V. C. M. Leung, and H. Yin, "Energy efficiency optimization for rate-splitting multiple access based indoor visible light communication networks," *IEEE J. Sel. Areas Commun.*, vol. 40, no. 5, pp. 1706–1720, May 2022.
- [41] S. A. Naser, P. C. Sofotasios, S. Muhaidat, and M. Al-Qutayri, "Rate-splitting multiple access for indoor visible light communication networks," in *Proc. IEEE Wireless Commun. Netw. Conf. Workshops*, 2021, pp. 1–7.
- [42] T. Komine and M. Nakagawa, "Fundamental analysis for visible-light communication system using LED lights," *IEEE Trans. Consum. Electron.*, vol. 50, no. 1, pp. 100–107, Feb. 2004.
- [43] Z.-G. Sun, H.-Y. Yu, Z.-J. Tian, and Y.-J. Zhu, "Linear precoding for MU-MISO VLC systems with noisy channel state information," *IEEE Commun. Lett.*, vol. 22, no. 4, pp. 732–735, Apr. 2018.
- [44] M. Grant and S. Boyd, "CVX: MATLAB software for disciplined convex programming," version 2.1, Mar. 2014. [Online]. Available: <http://cvxr.com/cvx/>
- [45] A. A. Ahmad, Y. Mao, A. Sezgin, and B. Clerckx, "Rate splitting multiple access in C-RAN: A scalable and robust design," *IEEE Trans. Commun.*, vol. 69, no. 9, pp. 5727–5743, Sep. 2021.
- [46] Y. Nesterov and A. Nemirovskii, *Interior Point Polynomial Methods in Convex Programming: Theory and Applications*. Philadelphia, PA: SIAM, 1994.
- [47] S. Tao, H. Yu, Q. Li, and Y. Tang, "Strategic analysis of user association based on power-domain non-orthogonal multiple access in visible light communication multi-cell networks," in *Proc. IEEE 19th Int. Conf. Commun. Technol.*, 2019, pp. 710–714.
- [48] C. Li, J. Zhang, and K. B. Letaief, "Energy efficiency analysis of small cell networks," in *Proc. IEEE Int. Conf. Commun.*, 2013, pp. 4404–4408.
- [49] Y. Hsiao, Y. Wu, and C. Lin, "Energy-efficient beamforming design for MU-MISO mixed RF/VLC heterogeneous wireless networks," *IEEE Trans. Signal Process.*, vol. 67, no. 14, pp. 3770–3784, Jul. 2019.
- [50] H. Shen, W. Xu, K. Zhao, F. Bai, and C. Zhao, "Non-alternating globally optimal MMSE precoding for multiuser VLC downlinks," *IEEE Commun. Lett.*, vol. 23, no. 4, pp. 608–611, Apr. 2019.